Eur. Phys. J. D **39**, 247–260 (2006)
DOI: 10.1140/epjd/e2006-00105-4

THE EUROPEAN PHYSICAL JOURNAL D

Spectral line shapes modeling in turbulent plasmas

Y. Marandet[1,a], H. Capes[2], L. Godbert-Mouret[1], M. Koubiti[1], J. Rosato[1], and R. Stamm[1]

[1] PIIM, Université de Provence, Centre de St-Jérôme, 13397 Marseille, France
[2] Association Euratom-CEA, CEA/DSM/DRFC, Centre de Cadarache, 13108 Saint-Paul-lez-Durance, France

Received 21 February 2005 / Received in final form 28 October 2005
Published online 18 May 2006

Abstract. In this work we investigate the influence of low frequency turbulence on Doppler spectral line shapes in magnetized plasmas. Low frequency refers here to fluctuations whose typical time scale is much larger than those characterizing the atomic processes, such as radiative decay, collisions and charge exchange. This ordering is in particular relevant for drift wave turbulence, ubiquitous in edge plasmas of fusion devices. Turbulent fluctuations are found to affect line shapes through both the spatial and time averages introduced by the measurement process. The profile is expressed in terms of the fluid fields describing the plasma. Assuming the spectrometer acquisition time to be much larger than the turbulent time scale, an ordering generally fulfilled in experiments, allows to develop a statistical formalism. We proceed by successively investigating the effects of density, fluid velocity and temperature fluctuations on the Doppler profile of a spectral line emitted by a charge exchange population of neutrals. Line shapes, and especially line wings are found to be affected by ion temperature or fluid velocity fluctuations, and can in some cases exhibit a power-law behavior. These effects are shown to be measurable with existing techniques, and their interpretation in each particular case would rely on already existing tools. From a fundamental point of view, this study gives some insights in the appearance of non-Boltzmann statistics, such as Lévy statistics, when dealing with averaged experimental data.

PACS. 32.70.Jz Line shapes, widths, and shifts – 52.35.Ra Plasma turbulence – 05.40.Fb Random walks and Levy flights

1 Introduction

Spectral line shape studies have played a major role in the investigation of the nature of atomic radiators and their environment, in astrophysics as well as in laboratory plasmas. Indeed, depending on the dominant line broadening mechanisms, it is for instance possible to retrieve the electron density or the ion temperature from the analysis of a given line. However, in many cases actual plasmas are far from thermal equilibrium, being inhomogeneous or having non-Maxwellian velocity distributions, features which significantly complicate the analysis of experimental data. In addition, these departures from thermal equilibrium can trigger instabilities, whose growth and non-linear saturation eventually lead to the onset of turbulence [1–3]. The importance of investigating the possible effects that turbulence might have on line shapes has been acknowledged very early, and the motivations of these studies were, and still are, two-fold: first there is the need to quantify the errors introduced by neglecting turbulence in routine diagnosis based on line-shapes. Then, the possible existence of significant deviations could be used to diagnose turbulence itself.

Historically, a large number of papers ([4,5] and references therein) have dealt with the Stark effect resulting from turbulent electric fields, such as those associated to a high supra-thermal level of Langmuir waves [6] or a low frequency microfield [7]. Starting from the seminal paper by Mozer and Baranger [8], several models have been devised to include turbulent Stark broadening in the calculation of line-shapes. The results thus obtained are relevant to plasmas for which Stark effect is dominant compared to Doppler effect. There are however situations for which this ordering is reversed, and important examples are edge plasmas of magnetic fusion devices such as Tokamaks in the ionizing regime. For these low density plasmas ($N_e \leq 5 \times 10^{20}$ m^{-3}), Zeeman and Doppler effects are the dominant broadening mechanisms for low lying lines such as the Dα (transition between the levels $n = 3$ and $n = 2$ of the atomic deuterium). In such cases, line shape studies essentially provide measurements of the emitters velocity distribution, and have so far brought valuable results concerning the origin of neutrals in edge plasmas [9–12]. However, these plasmas are known to be strongly turbulent, i.e. the level of fluctuation of the fluid fields characterizing the plasma can rise up to 30% [2,13,14]. The experimental characterization of these fluctuations is of first importance to analyse drift-wave (DW) turbulence,

[a] e-mail: yannick.marandet@piim.up.univ-mrs.fr

which is held responsible for the so called anomalous transport degrading the quality of the confinement [3]. The study of the Probability Density Functions (PDF) of the plasma fields is of particular interest since significant deviations from Gaussianity have been observed (e.g. [15]). The latter have serious consequences for plasma confinement, because they can markedly enhance turbulent transport. Various experimental techniques have been used to carry out turbulent fluctuations measurements, and are reviewed in reference [13]. Optical diagnostics have so far relied on active spectroscopy techniques, in particular on Beam Emission Spectroscopy (BES). The latter allows to diagnose the time behavior of turbulent density fluctuations at the edge of Tokamaks (e.g. [16,17]). Ion temperature and parallel velocity fluctuations have been measured using High Frequency Charge Exchange Recombination Spectroscopy (HF-CHERS) [14]. An optical diagnostic of turbulence based on passive spectroscopy would be very convenient, this comparatively simple technique being already available on numerous experiments. Moreover, passive spectroscopy is the only available technique in Astrophysics.

As an example, we will consider the case of the Balmer α of hydrogen isotopes (Dα for the case of deuterium), since it is one of the most routinely monitored line in edge plasmas, being both intense and optically thin. In Sections 2 and 3, the expression of the measured line profile is carefully discussed to emphasize the role of the spatial and time averages involved in the measure. We show in Section 2 that a neutral population created by charge exchange can be considered as being in a local equilibrium characterized by the local density, temperature and fluid velocity of the ions. In Sections 4 and 5, we show that in presence of low frequency turbulence, the Doppler profile gives access to an apparent velocity distribution. By further developing the model only briefly presented in [18,19], this apparent VDF is reexpressed in terms of the PDF of the fluid fields. In Section 6, the influence of density, fluid velocity and temperature are successively investigated in details. The experimental relevance of the results thus obtained is discussed. Finally, it is shown in Section 7 that for particular choices of the statistical properties of the turbulent fluctuations, the apparent VDF becomes a Lévy distribution. This result establishes a clear connection with one of our previous work [20], in which we investigated the possible origin of a power law behavior observed in the line wings of Dα spectra measured in the former ergodic divertor configuration of the Tore Supra Tokamak.

2 Expression of the measured spectra

Let us first define precisely the observable quantity for a spectrally resolved passive spectroscopy measurement. First of all, obtaining the spectrum emitted by the plasma (which will be referred to as the measured spectrum in the following) from the raw spectrum involves deconvolution of the apparatus function. In practice, the theoretical spectrum is convolved with the latter before being compared to the raw spectrum. The radiation emitted by the plasma is integrated both along the Line Of Sight (LOS) and during the acquisition time of the spectrometer, denoted by τ_m. The observable intensity $\mathcal{I}_{mes}(\Delta\lambda)$, where $\Delta\lambda$ stands for the wavelength detuning from the center of the line, is thus given by the following expression

$$\mathcal{I}_{mes}(\Delta\lambda) = \int_0^{\tau_m} \int_{\mathcal{L}} \mathcal{I}_{loc}(\Delta\lambda, z, t) \frac{\delta S}{4\pi z^2} dz\, dt, \quad (1)$$

where $\mathcal{I}_{loc}(\Delta\lambda, z, t)$ is the local line shape emitted at a given distance z from the detector along the LOS $\mathcal{L}$. Here δS stands for the detector active area. Assuming the latter to be delimited by $z_1 < z_2$ such that $L = z_2 - z_1 \ll z_1$, equation (1) reduces to

$$\mathcal{I}_{mes}(\Delta\lambda) \simeq \frac{\delta S}{4\pi z_1^2} \int_0^{\tau_m} \int_{z_1}^{z_2} \mathcal{I}_{loc}(\Delta\lambda, z, t) dz\, dt. \quad (2)$$

We now introduce the local absolute brightness

$$b(z,t) = \int_{-\infty}^{+\infty} \mathcal{I}_{loc}(\Delta\lambda, z, t)\, d\Delta\lambda, \quad (3)$$

and define the local line shape normalized to unity by $\mathcal{I}(\Delta\lambda, z, t) = \mathcal{I}_{loc}(\Delta\lambda, z, t)/b(z,t)$. In the remainder of this paper, we will deal with the measured profile normalized to unity, given by

$$\mathcal{I}_{mes}(\Delta\lambda) = \frac{1}{\tau_m} \int_0^{\tau_m} \frac{1}{L} \int_{z_1}^{z_2} B(z,t) \mathcal{I}(\Delta\lambda, z, t) dz\, dt. \quad (4)$$

where the relative brightness B is defined by

$$B(z,t) = \frac{b(z,t)}{(1/\tau_m)\int_0^{\tau_m} (1/L) \int_{z_1}^{z_2} b(z,t) dt dz}. \quad (5)$$

So, the measurement process both entails a spatial and a time average of the local profile. In order to achieve time resolved measurements, the acquisition time τ_m should be chosen shorter than the typical turbulent time, which is associated to the time variations of the functions $B(z,t)$ and $\mathcal{I}(\Delta\lambda, z, t)$. However, such a choice would generally result in spectra having very low signal to noise ratios. In this work we deal with the opposite situation, where the acquisition time is much larger than the typical turbulent time scale. In fact, this generally corresponds to the actual situation for passive spectral line shapes measurements. The next step in the modeling consists in relating the local brightness B and the local profile $\mathcal{I}$ to the parameters characterizing the plasma.

3 Modeling of the local profile

In this section we will first describe the model that will be used to describe the plasma, i.e. a set of fluid equations. The remainder of the section will present the expressions of the local brightness and profile relevant to edge plasmas typical conditions.

3.1 Plasma description

We are interested in plasmas which can be described by a set of N macroscopic fields φ_i, denoted in a shorthand way by

$$\varphi = \{\varphi_1(\mathbf{r},t),\ldots,\varphi_N(\mathbf{r},t)\}. \quad (6)$$

The latter set of fields includes the density, temperature and fluid velocity for each species. These fields are solutions of a set of fluid equations [21,22]. The fields $\varphi_i(\mathbf{r},t)$ obey conservation equations

$$\frac{\partial\varphi_i}{\partial t} + \nabla\cdot\mathbf{\Gamma}_i = S_i(\varphi), \quad (7)$$

where $S_i(\varphi)$ is a source term, and $\mathbf{\Gamma}_i$ is a flux. The latter is given by the sum of a diffusive and a convective flux $\mathbf{\Gamma}_i = -\kappa_i(\varphi)\nabla\varphi_i + \mathbf{u}\varphi_i$, where $\mathbf{u} = \varphi_j$ is a velocity field and $\kappa(\varphi)$ is the diffusion coefficient for the field φ_i. It is furthermore assumed that this set of fluid equations describes a turbulent stationary state, for which the statistical properties of the plasma do not change during the acquisition time τ_m. For each species, the validity of the fluid description relies on the orderings $\tau \gg \nu_{coll}^{-1}$ and $\Lambda \gg \lambda_{coll}$, where τ (resp. Λ) is the typical time (resp. length) scale of variation of the fluid fields, ν_{coll} the collision frequency and λ_{coll} the mean free path. In the case of DW turbulence in edge plasmas, we have $\tau \sim$ 10–100 μs and $\Lambda \sim 1$ cm [13]. These orderings ensure that both the electrons and ions VDF remain close to a local Maxwellian at each time and location [21,22], that is

$$F(\mathbf{v},\mathbf{r},t) \simeq \left(\frac{m}{2\pi T(\mathbf{r},t)}\right)^{3/2} \exp\left(-\frac{m(\mathbf{v}-\mathbf{u}(\mathbf{r},t))^2}{2T(\mathbf{r},t)}\right), \quad (8)$$

where m, $T(\mathbf{r},t)$ and $\mathbf{u}(\mathbf{r},t)$ are respectively the mass, the temperature field expressed in eV, and the fluid velocity field of either electrons or ions.

The calculation of the neutrals VDF requires the use of a refined model. Indeed, there are different sources of neutrals in edge plasmas of Tokamaks, each of them giving birth to a single class of neutrals. These classes, characterized by different temperatures, coexist since the density is usually too low in order to ensure their complete relaxation toward the background local equilibrium. The lowest temperature class originates from the dissociation of molecules released from the wall, whereas those having larger temperatures are mainly attributed to charge exchange reactions (e.g. [9–12]). In the following, we will only consider the class of neutrals locally created by charge exchange reactions, which plays an important role for the line wings behavior. Indeed, it will be shown that turbulence affects these regions of the spectra. In order to model the VDF of these emitters, we can once again take advantage of the separation of scales between atomic processes and turbulence. In fact, the inverse of the charge exchange rate is of the order of a few μs [23], i.e. shorter than the typical turbulent time scale. As a result, the emitters VDF remains at each time close to that of the ions, given by equation (8). From the microscopic point of view, the emitter's VDF thus appears as a Maxwellian characterized by a set of slowly varying macroscopic fields.

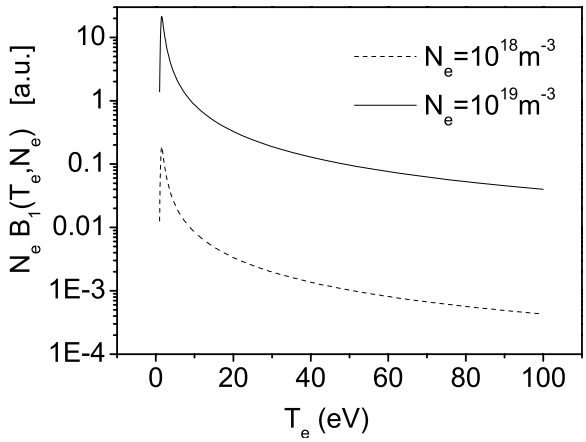

Fig. 1. Plot of the brightness per emitter times the electron density as a function of the electronic temperature on a logarithmic scale, for two densities $N_e = 10^{18}$ m^{-3} and $N_e = 10^{19}$ m^{-3}. The temperature dependence is weak for $T_e > 15$ eV.

3.2 The local brightness

The local line brightness is directly related to the population of the transition upper atomic level. In general, this population has to be calculated by taking into account the contributions of the different processes (for instance collisions, charge exchange, radiative decay) populating or depopulating the levels. If the fluid fields characterizing the plasma vary slowly on the typical time scales associated to these processes, a stationary approach is suitable to calculate the brightness. The levels populations are assumed to be time independent and are calculated using the values of the fields $\varphi(\mathbf{r},t)$ at each time and location. In practice, the brightness essentially depends on the electron density $N_e(\mathbf{r},t)$ and temperature $T_e(\mathbf{r},t)$. We have performed a calculation of the brightness per emitter B_1 (defined as $B(\mathbf{r},t) = N_0(\mathbf{r},t)B_1(\varphi(\mathbf{r},t))$, where $N_0(\mathbf{r},t)$ is the density of emitters) for the Dα line in edge plasma conditions, i.e. $N_e = 10^{18}$–10^{19} m^{-3} and T_e = 1–100 eV, using the code SOPHIA [24]. The electron density dependence of B_1 is found to be linear, in accordance with the fact that the upper level of the transition is essentially populated by electronic collisions from the ground state. This leads to a quadratic behavior of the brightness with N_e, since $N_0 \propto N_e$. The influence of the electron temperature on the brightness is more subtle, as shown in Figure 1 for two different densities. The existence of a maximum reflects the competition between the growth of the electron collisions cross-section with temperature, which dominates the small temperatures behavior, and the ionisation process. For electron temperatures larger than 15 eV, the influence of T_e on the brightness is weak, and in the remainder of this paper,the brightness will be treated as a function of the electron density only.

3.3 The local line shape

The $\Delta\lambda$ dependence of the local profile $\mathcal{I}(\Delta\lambda, z, t)$ is determined by the dominant line broadening mechanisms. In magnetized plasmas, Zeeman, Stark and Doppler broadenings should a priori be taken simultaneously into account. In general, the local profile normalized to unity can be written as the following convolution product

$$\mathcal{I}(\Delta\lambda, z, t) = \int d\Delta\lambda' I_{ZS}(\Delta\lambda - \Delta\lambda', z, t) I_D(\Delta\lambda', z, t), \tag{9}$$

where I_{ZS} is the local Zeeman-Stark profile, which describe the broadening resulting from the effect of the magnetic and electric fields on the emitters energy levels [4]. The Doppler profile I_D is related to the wavelength shift introduced by the movement of the radiator along the LOS, and is thus directly given by

$$I_D(\Delta\lambda, z, t) d\Delta\lambda = f(v_z, z, t) dv_z, \tag{10}$$

where $f(v_z, z, t)$ stands for the emitters VDF along the LOS, obtained from (8) upon integrating over the two components of the velocity perpendicular to the LOS

$$f(v_z, z, t) = \iint dv_x dv_y F(\mathbf{v}, z, t). \tag{11}$$

It should be noted that equation (10) would not be valid if the velocity of the emitter were not constant because of the collisions during the emission process [25]. If $\Delta\omega_D$ denotes the Doppler line width expressed in units of pulsation, equation (10) assumes that $\tau_{coll}^{-1} \ll \Delta\omega_D$. This ordering is largely satisfied in edge plasmas, and is moreover not inconsistent with the assumption $\tau_{col} > \tau$ underlying the validity of equation (8). For a given line, the relative importance of the different broadening mechanisms depends on plasma conditions, i.e. on the average values taken by the plasma density and temperature, but also on the detuning $\Delta\lambda$. In the following, we will again discuss the case of the Dα line, first for the bulk of the line and then for line wings, which are the regions of the spectra defined by $|\Delta\lambda| \gg \Delta\lambda_{1/2}$, $\Delta\lambda_{1/2}$ being the HWHM (Half Width at Half Maximum) of the profile. In the center of the line, Stark effect is negligible for densities lower than $N_e = 5 \times 10^{20}$ m^{-3}, an ordering which is usually (but not always) satisfied in edge plasmas. In addition, since the magnetic field is larger than 1 T, fine structure can be neglected [26]. Therefore, the Dα line splits into three Doppler-broadened Zeeman components (one π and two σ). The lateral σ components are equally separated from the central π component. Under parallel observation with respect to the magnetic field, only the σ components are observable. Although negligible in the bulk of the line, Stark effect might become dominant in the line wings for detunings larger than a value $\Delta\lambda_S(N_e)$ which is an increasing function of the density. Therefore, in the remainder of the paper it should be understood that the Doppler line wings are the regions of the spectra for which both orderings $|\Delta\lambda| \gg \Delta\lambda_{1/2}$ and $|\Delta\lambda| < \Delta\lambda_S$ are simultaneously valid. The existence of such a regime depends on the plasma conditions. Its study is relevant in the range of plasma parameters considered here [27], and consequently Stark effect will be neglected. However, it should be emphasized that the statistical formalism which is developed in Section 5 would also be applicable if Stark effect were not negligible. In the latter case, the local profile should be calculated using equation (9) instead of equation (10).

According to equation (10), the Doppler spectrum of a single Zeeman component is proportional to the emitters VDF f along the line of sight. As previously explained, we consider a class of neutrals created by charge exchange reactions, whose VDF is approximated by a local Maxwellian. The corresponding expression of the local Doppler profile is given by

$$\mathcal{I}_D(\Delta\lambda, \mathbf{r}, t) = \sqrt{\frac{m}{2\pi T(\mathbf{r}, t)}} \exp\left(- \frac{\left(\Delta\lambda - \frac{\lambda_0}{c} u_z(\mathbf{r}, t)\right)^2}{\frac{2\lambda_0}{mc} T(\mathbf{r}, t)} \right), \tag{12}$$

where m is here the emitters mass, λ_0 the unperturbed wavelength of the transition under study, c the speed of light, $T(\mathbf{r}, t)$ the ion temperature, and $u_z(\mathbf{r}, t)$ the component of the ion fluid velocity along the LOS.

4 Apparent velocity distribution

Gathering the results of the sections above, we obtain the following expression for the measured profile normalized to unity

$$\mathcal{I}_{mes}(\Delta\lambda) = \frac{1}{\tau_m} \int_0^{\tau_m} dt \frac{1}{L} \int dz\, B(\varphi(z,t)) I_D(\Delta\lambda, \varphi(z,t)), \tag{13}$$

which is now expressed in terms of the fluids fields describing the plasma. The *apparent velocity distribution function* $f_a(v_z)$ is straightforwardly deduced from the measured spectrum by

$$\mathcal{I}_{mes}(\Delta\lambda) d\Delta\lambda = f_a(v_z) dv_z, \tag{14}$$

in analogy with equation (10). This VDF is an average of the local emitters VDF over time and space. Indeed, combining equation (13) and equation (14) leads to the following explicit expression

$$f_a(v_z) = \frac{1}{\tau_m} \int_0^{\tau_m} dt \frac{1}{L} \int dz\, B(\varphi(z,t))\, f(v_z, \varphi(z,t)). \tag{15}$$

The apparent VDF f_a can be given a deep physical meaning as will be shown in Section 7.

Intuitively, in plasmas where the fluctuation rate is low, f_a should remain close to a Maxwellian f_{eq} characterized by the time and space averaged values of the temperature and the velocity fields, respectively denoted by T_0 and u_{z0}, i.e.

$$f_a(v_z) \simeq f_{eq}(v_z; T_0, u_{z0}). \tag{16}$$

Conversely, in a situation where strong fluctuations occur, there is a priori no obvious reason for which the apparent velocity distribution should remain close to the average Maxwellian given by equation (16). In particular, in edge plasmas the fluctuation rate can rise up to several tens of percents. The validity of equation (16) then clearly becomes questionable, and equation (15) should be used instead. A calculation of the apparent VDF f_a can be carried out from the latter equation once the solutions of the fluid equations are known, i.e. the time and space dependences of each of the fields $\varphi_i(\mathbf{r},t)$ have been worked out. Because of the non-linear nature of the fluid equations and the complexity of the geometry, this calculation would best be achieved numerically. Although such an approach might be able to encompass the complexity of the problem, we find it worthwhile to begin with a simpler one in order to gain insights on the kind of effects that turbulence might produce on spectral line shapes.

5 Statistical formalism

5.1 Expression of the profile

In the following, we will take advantage of the fact that the acquisition time of the spectrometer is usually much larger than the typical time scale of the turbulence τ. Let us first note that upon using an appropriate normalisation for the δ function, the following relation holds for any z and t

$$\int_N \prod_{i=1}^{N} \delta(\Phi_i - \varphi_i(z,t)) d\Phi_1 ... d\Phi_N = 1, \tag{17}$$

where Φ_i is the sample space variable corresponding to the value of the field φ_i at point (z,t). Introducing this identity into equation (15), interchanging the order of time and sample space integrations, and finally making use of the delta function sifting property yields the following expression for the apparent velocity distribution function

$$f_a(v_z) = \int \frac{dz}{L} \int d\Phi \overline{\delta(\Phi - \varphi(z,t))} B(\Phi)\, f(v_z,\Phi). \tag{18}$$

The bar denotes a time average of the delta functions product, and is time independent because of the stationarity assumption. This is by definition the joint Probability Density Function (PDF) of the fields φ_i at point z, denoted by

$$\mathcal{P}(\Phi_1,\cdots,\Phi_N,z) = \overline{\prod_{i=1}^{N} \delta(\Phi_i - \varphi_i(z,t))}. \tag{19}$$

The apparent VDF becomes

$$f_a(v_z) = \frac{1}{L} \int_{\mathcal{L}} dz \int d\Phi \mathcal{P}(\Phi,z) B(\Phi)\, f(v_z,\Phi), \tag{20}$$

and finally, upon integrating on the space coordinate z, the apparent VDF is given by

$$f_a(v_z) = \int d\Phi W(\Phi) B(\Phi)\, f(v_z,\Phi), \tag{21}$$

where the spatially integrated PDF $W(\Phi)$ is obtained from

$$W(\Phi) = \frac{1}{L} \int dz \mathcal{P}(\Phi,z). \tag{22}$$

In the remainder of the paper we shall furthermore assume homogeneous turbulence along the line of sight, that is $W(\Phi) \equiv \mathcal{P}(\Phi,z)$. In edge plasmas, this requires that the size of the emitting zone should be small with respect to the gradient length. This is more likely to be the case when the line of sight is parallel to the magnetic field lines, even though radial gradients could induce sufficient radial localization of the emission. To conclude on this, let us emphasize that the role of time and space are symmetric, and that instead of a time average we could have introduced space averages. In the case where turbulence is both stationary and homogeneous the two averages can equivalently be introduced.

In the following, we will use a stochastic model for turbulence, the fields φ being considered as random functions. In this case it is interesting to convert the time average in equation (19) to an ensemble average. The inequality $\tau \ll \tau_m$, where τ is the typical time characterizing turbulent fluctuations, justifies the use of the following ergodic theorem [28]

$$\lim_{\tau_m \to +\infty} \frac{1}{\tau_m} \int_0^{\tau_m} \delta(\Phi - \varphi(z,t)) dt = \langle \delta(\Phi - \varphi(z,t)) \rangle\,, \tag{23}$$

where $\langle\cdot\rangle$ denotes the ensemble average. This reformulations allows to make contact with the results of the Sinai model, to be presented later on.

5.2 Discussion

In the frame of our statistical reformulation, it is no longer necessary to know the solutions of the fluid equations in order to calculate the apparent VDF. Instead, the joint PDF of the turbulent fields should have been computed. A straightforward approach would be to rely on a fluid code, so as to compute histories of the different fields, and then their PDF. As we have already pointed out, this would require heavy numerical computation, especially in order to obtain the PDF tails with a good accuracy. Furthermore, if such calculations were carried out, any statistical reformulation would obviously be superfluous, and the apparent VDF could directly be obtained from equation (15). An approach more suited to our formalism should proceed directly at the PDF level. Formalisms allowing to calculate turbulent fluctuations PDFs are however not yet very well developed, for a review see reference [1]. Dealing with a realistic set of coupled fluid equations is out of reach at the present time, and work in this direction has been limited to the simplest plasma turbulence models, such as the Hasegawa-Mima equation [29]. The next section will nevertheless be devoted to present one of the most studied approach, initially developed by Pope [30]. The results thus obtained for the ion temperature PDF should not be understood as encompassing the complexity of Tokamak edge plasmas turbulence. Their interest is

to shed some light onto what governs the PDF shape in a simplified model. Calculations of the apparent VDF for different values of the model parameters will then allow to draw conclusions on the properties that turbulence should have so as to significantly affect line shapes. This is the main advantage of our statistical reformulation.

5.3 Determination of the PDF from the fluid equations

Let us consider the passive advection of a scalar $\varphi(z,t)$ solution of equation (7), in which the source term is an arbitrary function of φ and the flux $\mathbf{\Gamma}$ is the sum of a convective term and a diffusive term. The convective velocity field $\mathbf{u}$ is assumed to be a stochastic field, the statistical properties of which are known. In edge plasmas $\mathbf{u}$ would be the electric drift velocity, which is divergence free to a good approximation. In order to calculate the apparent velocity distribution function from equation (21), the spatially integrated joint PDF of velocity and temperature, denoted by $W(\mathbf{u},\Phi)$, should be calculated. Here, we will limit ourselves to the modeling of the marginal distribution $W(\Phi)$, obtained by integrating $W(\mathbf{u},\Phi)$ over the velocity. Indeed, this will be sufficient to highlight the salient points of the model. Assuming homogeneous turbulence, and then following Pope [30], the time dependent PDF $W(\Phi,t)$ is shown to obey a Fokker-Planck like equation with a negative diffusion coefficient

$$\frac{\partial W}{\partial t} = \frac{\partial}{\partial \Phi}[S(\Phi)W] - \frac{\partial^2}{\partial \Phi^2}[D(\Phi)W], \qquad (24)$$

where $S(\Phi)$ is the source term in the fluid equation. The expression of the function $D(\Phi)$ will be discussed below. The stationary solution of the latter equation is

$$W(\Phi) = \frac{C}{D(\Phi)} \exp\left(-\int_0^{\Phi} \frac{S(w)}{D(w)} dw\right). \qquad (25)$$

As a result, in the PDF approach a non-linear source term S does not introduce any closure problem, unlike in the moment based models [1]. The problem remains nonetheless unclosed, since the function $D(\Phi)$ is in general not expressible in terms of $W(\Phi)$ or $S(\Phi)$ alone. Indeed, the shape of this function depends on the correlations between Φ and its gradient. More precisely, it can be recast in the following form

$$D(\Phi) = \frac{1}{\langle \nabla\Phi \rangle^2} \int d(\nabla\Phi) \mathcal{P}(\nabla\Phi|\Phi)(\nabla\Phi)^2, \qquad (26)$$

where $\mathcal{P}(\nabla\Phi|\Phi)$ is the PDF of the gradient of Φ, conditioned to a given value of Φ [30]. In order to obtain this PDF, an equation for the joint PDF of Φ and its gradient should be written [31], which in turn would involve correlations with higher orders gradients. Eventually, one ends up with an infinite hierarchy of equations, involving the joint PDFs of $\Phi, \nabla\Phi, \nabla^2\Phi, ...$ In addition, it should be kept in mind that the statistical properties of the velocity field $\mathbf{u}$, while not appearing explicitly in equation (25), do actually affect the shape of $D(\Phi)$ through equation (7), as should the expression of $S(\Phi)$. The closure of this hierarchy has proven to be difficult to address, and is largely beyond the scope of the present work [1]. For our purposes it will be sufficient to present an early attempt to this closure problem, due to Sinai and Yakhot [32], which leads to results consistent with subsequent findings based on refined analysis [33,34]. Their work deals with passive advection of temperature in homogeneous decaying turbulence, for which there is no source term in the temperature equation. The quantity of interest is $X = (T - T_0)/\sigma$, where $\sigma^2 = \langle T^2 \rangle - T_0^2$. The field X obeys an equation analogous to equation (7), $S(X)$ being a linear function of X. The following Taylor development is used to express the function $D(X)$

$$D(X) \simeq 1 + kX^2, \qquad (27)$$

where the parameter $k \geq 0$ is a measure of the correlations strength. Taking the limit $k \to 0$ is equivalent to neglect correlations altogether, and leads to a Gaussian PDF of variance σ according to equation (25). A non linear source term $S(X)$ would however preclude Gaussianity even in the correlation free case. When $k > 0$, the following result for the temperature PDF is readily obtained

$$W(T) \simeq \frac{C}{\left(1 + k\left(\frac{T-T_0}{\sigma}\right)^2\right)^{1+1/2k}}, \qquad (28)$$

where C is a normalization constant, σ controls the width of the distribution, and $\langle T \rangle \simeq T_0$. Figure 2 shows a plot of $W(T)$ for $T_0 = 30$ eV, $k = 10$ and $\delta T/T = \sigma/T_0 = 10$, 20, 30%. A few subtleties and limitations concerning the use of this result deserve to be mentioned. First, it should be noted that σ is actually time dependent. We shall assume here that the acquisition time τ_m is chosen such that $\sigma/\dot{\sigma} \ll \tau_m$. This requires a separation of time scales between the turbulent fluctuations and the decay of the average quantities. Secondly, the correlations are treated using the development given by equation (27), should only be valid for values of the temperatures such that $|X| \ll 1$.

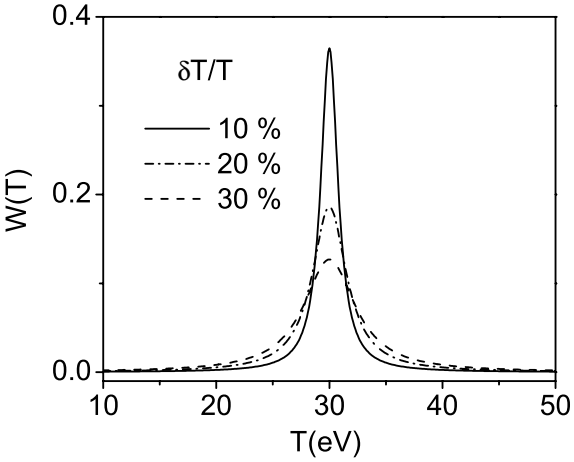

Fig. 2. Plot of the Sinai PDF for $T_0 = 30$ eV, $k = 10$ and for different values of the fluctuation rate $\delta T/T = 10$, 20, 30%.

However, as pointed out in reference [32], comparison to numerical simulations have shown that the range of validity of equation (28) is much wider than expected, being such that $|X| \leq 7$. It should be pointed out that the distribution given by equation (28) is a Tsallis distribution (e.g. [35]) with $q = (1 + 2k)^{-1}$. Therefore, in this model, temperature fluctuations obey Tsallis nonextensive statistical mechanics [35] when correlations exist, and Boltzmann statistics for vanishing correlations.

In the next section, we shall use these results as an input for apparent VDF calculations.

6 Application to the case of one fluctuating variable

In an actual turbulent plasma, several fields fluctuate, and these fluctuations are coupled. According to equation (21), the joint PDF of the relevant fields should be computed in order to calculate the apparent VDF. However, the role of density, velocity and temperature fluctuations on the apparent VDF shape have no reason to be identical. As a first approximation, it is therefore useful to consider the idealized case in which only one field fluctuates. This will shed light on which field fluctuations lead to the most significant effects on line shapes.

6.1 Density fluctuations

Let us first consider density fluctuations. Since the local VDF normalized to unity does not depend on density, the integration over density fluctuations is trivially performed, and the apparent VDF is found to be equal to the local emitters VDF

$$f_a(v_z) = \int_0^{+\infty} dn\, B(n) W(n) f(v_z, T_0) = f(v_z, T_0), \quad (29)$$

where T_0 is the constant plasma temperature. Therefore, at this level of approximation, Doppler line shapes are not sensitive to density fluctuations. The apparent VDF should thus remain Gaussian with the temperature T_0, whatever the shape of $W(n)$. This is in sharp contrast with line brightness time resolved measurements, which essentially provide information on density fluctuations. However, it should be noted that for cases in which Stark effect is not negligible, equation (29) no longer holds, since the local line shape then strongly depends on the density. As we have already pointed out, the formalism presented here could nevertheless be used upon replacing the local Doppler profile by the total profile given by equation (9). This will be the subject of further work.

6.2 Fluid velocity fluctuations

Let us now investigate the case in which only the fluid velocity fluctuates. In the following, $W(u_z)$ stands for the PDF of the fluid velocity component $u_z = \mathbf{u} \cdot \hat{z}$ along the line of sight (Oz), and σ_{uz}^2 for its variance. Changing the orientation of the line of sight therefore allows to fully investigate anisotropic velocity fields. Starting from equation (21), the apparent VDF reduces to

$$f_a(v_z) = \int W(u_z) f(v_z - u_z, T_0)\, du_z, \quad (30)$$

which is the convolution product of W and the local Maxwellian characterized by the constant plasma temperature T_0. Equation (30) is a well-known result in plasma spectroscopy, which is mentioned in classical textbooks [36]. A shape-independent definition of the apparent temperature T_a from the profile should proceed from its second moment

$$\xi T_a = \int_{-\infty}^{+\infty} f_a(v_z) v_z^2 dv. \quad (31)$$

In the fluctuations-free case, the actual temperature of the emitters T_0 is recovered, whereas if fluctuations do occur the apparent temperature is given by

$$T_a = T_0 \left[1 + \frac{\sigma_{uz}^2}{v_{th}^2} \right], \quad (32)$$

where v_{th} is the thermal velocity corresponding to the temperature T_0. The apparent temperature obtained from the Doppler line width is thus not rigorously equal to the actual temperature of the emitters. This result has already been mentioned by several authors, and was actually used in the first models retaining the effect of turbulence on Doppler line shapes in astrophysics [37]. To estimate the extent to which T_a might differ from T_0 in edge plasmas, we first have to specify the orientation of the line of sight. Indeed, the statistical properties of the component of the velocity perpendicular to the magnetic field $\mathbf{u}_\perp$ can significantly differ from that of the parallel velocity $u_\parallel$. For the perpendicular velocity $\mathbf{u}_\perp \sim \mathbf{E} \times \mathbf{B}/B^2$ we use a standard mixing length approximation, which gives $\sigma_{u\perp}/v_{th} \sim k_\perp L_\perp \lesssim 0.3$ where $k_\perp$ is the typical wave number for fluctuations and $L_\perp$ the macroscopic gradient length. The parallel velocity fluctuations rates where found to be of the order of 1% in reference [14] for TFTR supershot discharges. However, there are situations where parallel velocity fluctuations might be larger, in particular when driven by a Kelvin-Helmholtz like instability. In any case, it is reasonable to assume $\sigma_{u\parallel} \lesssim \sigma_{u\perp}$. Hence, $\sigma_{uz}/v_{th} \lesssim 30\%$ leading to $(T_a - T_0)/T_a \lesssim 10\%$, which roughly equals the uncertainty introduced by the fitting procedure. This estimation suggests that the Dα line width is not strongly modified by fluid velocity fluctuations. However, as pointed out in reference [36], this effect would be stronger for heavy emitters of mass M, because their thermal velocity is smaller ($v_{th} \propto M^{-1}$). This suggests that the so called impurity lines in fusion plasmas are more sensitive to turbulent velocity fluctuations. Now, considering only the line width is not sufficient since the PDF $W(u_z)$ might be non Gaussian. In fact, recent findings in astrophysical spectra [38–40], as well as

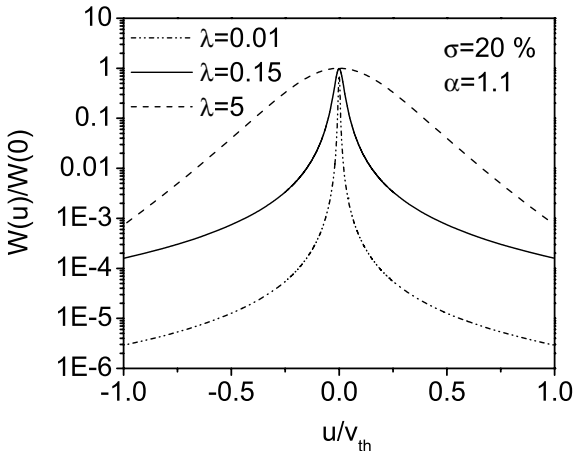

Fig. 3. Plot of the truncated Lévy velocity PDF for $\alpha = 1.1$, $\sigma = 0.2$ for $\lambda = 0.01$ (dash-dotted line), $\lambda = 0.15$ (solid line), $\lambda = 5$ (dashed line). The fluid velocity is plotted in units of the thermal velocity v_{th}, and each PDF is divided by its value at the origin. The transition from a Gaussian behavior (parabola for $\lambda = 5$) to the Lévy behavior ($\lambda = 0.01, 0.15$, concave in log-linear scale, signaling slower than exponential decay) is clearly seen. For v/v_{th} large enough, i.e. ~ 10 the PDF calculated for $\lambda = 0.01$ eventually proves to have the slowest decay.

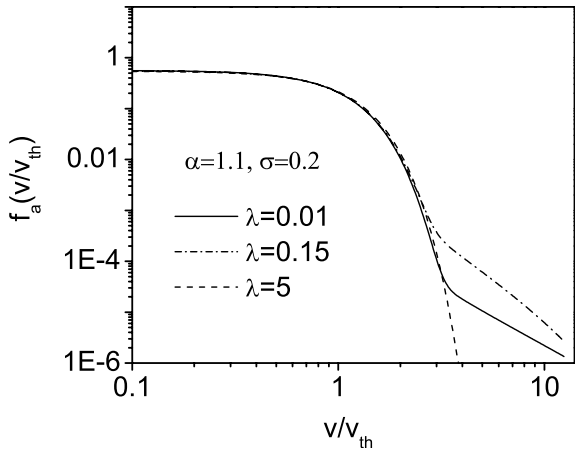

Fig. 4. Plot of the apparent velocity distribution corresponding to a truncated Lévy velocity PDF in a logarithmic scale. The velocity is plotted in units of the thermal velocity v_{th}. For $\lambda = 5$ the apparent VDF is very close to a Gaussian and turbulence only leads to a barely noticeable 4% increase in the line width. In the opposite case where $\lambda = 0.01$ the existence of an algebraic decay of exponent $-\alpha + 1$ in the tail of the apparent VDF is clearly seen. For $v/v_{th} < 10$, the intermediate case $\lambda = 0.15$ gives rise to the most significant effects.

in Tokamak plasmas for poloidal electric fields (hence radial velocity fluctuations) [15], indicate strong deviations from the Maxwellian, especially for line wings. As an illustration, let us consider PDFs corresponding to truncated Lévy flights, which were fitted to experimental data in the latter reference. These PDFs, which have finite variance, are defined in Appendix A. Depending on the value of the cutoff parameter λ, they either exhibit overall Gaussian or Lévy behavior. This is seen in Figure 3, where $W(u)/W(0)$ is plotted as a function of u/v_{th} for $\sigma_u/v_{th} = 20\%$, $\alpha = 1.1$ and $\lambda = 0.01, 0.15, 5$. When λ is decreased, the tails of the PDF become fatter and its FWHM decreases in concert because the variance is kept constant. As a result, for a given variance, the fatter the tails of the fluctuation PDF, the less affected the bulk of the line. The converse is true for the apparent VDF tails (i.e. line wings), as shown in Figure 4.

However, it should be pointed out that for this effect to be observable, large amplitude velocity fluctuations of the order of a few thermal velocity v_{th} should actually occur. Such fluctuations are therefore more likely to be observed in astrophysics, where turbulence has a looser meaning, i.e. that of unresolved movements.

6.3 Temperature fluctuations

Finally, we consider the case where only the ion temperature fluctuates, and for which the apparent VDF reads

$$f_a(v_z) = \int_0^{+\infty} W(T) f(v_z, T) dT. \tag{33}$$

The latter is not a convolution product, in opposition to the case of velocity fluctuations. To begin with, the apparent temperature defined by equation (31), is given by

$$T_a = \int_0^{+\infty} dT\, W(T) T = T_0, \tag{34}$$

and is therefore equal to the mean temperature of the distribution $W(T)$. Hence, the apparent temperature T_a always corresponds to the average temperature of the plasma ions, regardless of the PDF shape. This general and simple result concerning the apparent VDF f_a width contrasts with what is obtained for its shape. Indeed, f_a is given by a weighted sum of Gaussians of different widths, and cannot be Gaussian itself. For a temperature PDF sharply peaked around T_0, the actual deviations from Gaussianity are not expected to be very significant, because the dominant contribution in the integral of equation (33) comes from the neighborhood of T_0. In the limit where $W(T) = \delta(T - T_0)$, the Maxwellian with temperature T_0 is recovered. This line of argument breaks down if the width of the temperature PDF becomes too large, but also for large velocities ($v_z > v_{th}$) even for moderate fluctuations rates. Indeed, the value of $f(T_0, v_z)$ scales with v_z as

$$f(T_0, v_z) \propto \exp\left(-\frac{v_z^2}{\xi T_0}\right), \tag{35}$$

and therefore strongly decreases as v_z increases. Consequently, as shown in Figure 5, the contribution of the maximum of the temperature PDF in the integral becomes negligible for large enough v_z. Therefore, the largest deviations from Gaussianity are expected to appear in the apparent VDF tails, i.e. line wings. The actual extent of these deviations depend on the fluctuation level, but most importantly on $W(T)$ shape. As a rule of thumb, the slowest its asymptotical decay, the largest the deviations.

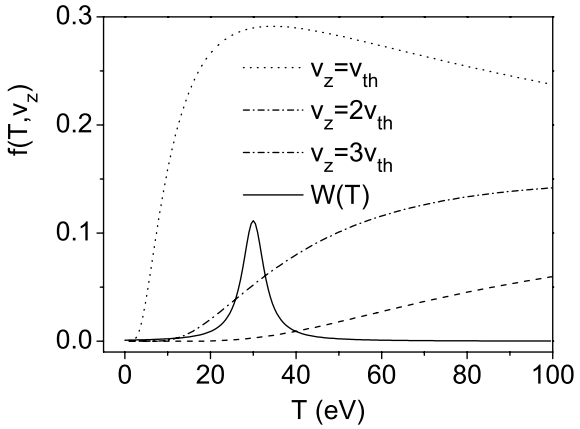

Fig. 5. Plot of the local VDF $f(T, v_z)$ as a function of T for three different values of the component of the velocity along the LOS $v_z = v_{th}$, $2v_{th}$, $3v_{th}$, where v_{th} is the thermal velocity for 30 eV. A model distribution $W(T)$, peaked around $T_0 = 30$ eV is also plotted (solid line). As v_z is increased, the contribution of T_0 in the calculation of the apparent VDF becomes all the more negligible than the tail of $W(T)$ decreases slowly.

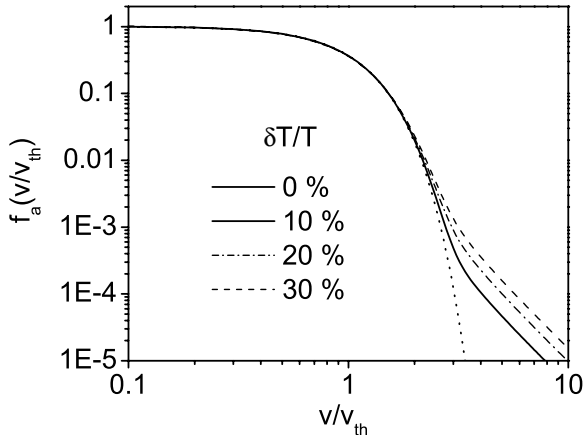

Fig. 6. Plot of the apparent VDF on a logarithmic scale for the Sinai PDF with $k = 10$ and the following values of the fluctuation rate $\delta T/T_0 = 10$, 20, 30%. These PDFs are plotted on Figure 2. v_{th} stands for the thermal velocity for $T_0 = 30$ eV. These plots show the asymptotic power law behavior. The value of the exponent is –3.2 here. The dotted line corresponds to the Gaussian Doppler profile at the average temperature. The deviations from this Gaussian profile becomes more and more important as σ grows.

For instance, an algebraic behavior for the temperature PDF implies a similar one for the measured profile. The relation between the exponents can be obtained in the following manner, noting that for large velocities the apparent VDF can be approximated by

$$f_a(v_z) \sim \int_{v_z^2/\xi}^{+\infty} W(T) \frac{1}{\sqrt{T}} dT. \tag{36}$$

Using then a power-law ansatz for the temperature PDF, the following result is readily obtained

$$W(T) \propto \frac{1}{T^{\alpha+1}} \Longleftrightarrow f_a(v_z) \propto \frac{1}{|v_z|^{2\alpha+1}}. \tag{37}$$

For example, let us consider the case in which the temperature fluctuations PDF is the Sinai distribution given by equation (28), and plotted in a logarithmic scale in Figure 6 for $k = 10$, and for different values of $\delta T/T_0$ ranging from 10 to 30%. The bulk of the apparent VDF remains very close to that of the Maxwellian at 30 eV (dotted line) for every value of σ. However, the discrepancies become important in the apparent VDF tails (i.e. Doppler line wings), all the more so σ is increased. In addition, the tails are found to exhibit a linear behavior in logarithmic scale, which signals the expected power-law dependence. The value of the exponent which characterizes this algebraic decay is $-3 - 2/k$ in accordance to equation (37). The k dependence can be checked on Figure 7 where the apparent VDF is plotted for $\delta T/T_0 = 20\%$ and for different values of k ($k = 0.5$, 2, 10), i.e. different correlation strengths. The stronger the correlations, the larger the deviations from the Maxwellian. For $k > 2$, the apparent VDF depends only weakly on the value of k, but then when k becomes smaller than one, the deviations from the Maxwellian diminish quickly. In the Sinai model, the temperature PDF becomes Gaussian in the limit of vanishing correlations, i.e. $k \to 0$. The corresponding apparent

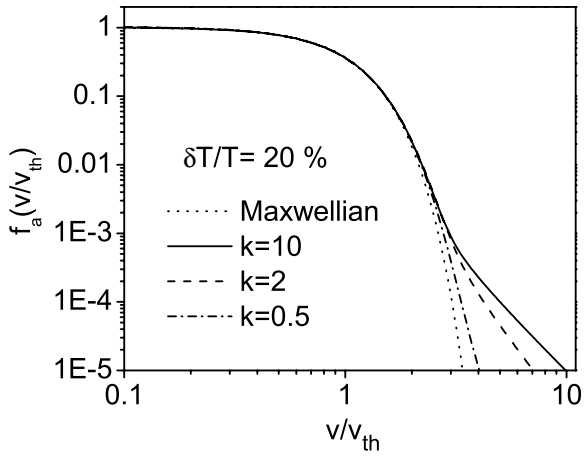

Fig. 7. Plot of the apparent VDF on a logarithmic scale for a fluctuation rate $\delta T/T_0 = 10\%$, and for different values of k, $k =$ 0.5, 2, 10. The values of the exponents characterizing algebraic decay of the tails are respectively 7, 4 and 3.2. The dotted line corresponds to the Gaussian Doppler profile characterized by a thermal velocity v_{th}.

VDF turns out to be indistinguishable from the average Maxwellian over 5 orders of magnitude. Hence, Gaussian fluctuations with $\delta T/T_0 = 20\%$ leave the line shape practically unchanged. This somewhat surprising result given the fluctuation rate, shows that characterizing temperature fluctuations solely by their variance is not sufficient to estimate the resulting effects on Doppler line shapes. It confirms the validity of the general results drawn from the analysis of equation (33) in the special case of the Sinai model, i.e. that long tails for the temperature PDF lead to modifications in the line wings.

In the frame of the Sinai model, the exponent α characterizing the apparent VDF power law decay is larger than 3. Other turbulence models could lead to smaller exponents. Let us indeed investigate the case in which the temperature PDF is a Lévy distribution of indexes $0 < \alpha < 1$ and $\beta = -1$, denoted by $\mathcal{L}_{\alpha,-1}(T)$ (see Appendix A). In this case $W(T) \equiv 0$ for negative arguments, as should be for the temperature field. The variance of one sided Lévy distributions can be made finite by introducing a cutoff, like in the symmetric case [41]. In the following, we consider the cut-off parameter λ to be small enough so that the PDF has a Lévy behavior over the whole range of interest while having finite moments. The Fourier transform $\tilde{f}_a(k)$ of the apparent VDF is given by

$$\tilde{f}_a(k) = \int_0^{+\infty} \mathcal{L}_{\alpha,-1}(T) \exp\left(-\frac{\xi T}{4}k^2\right) dT, \qquad (38)$$

and can be calculated explicitly using the following result [42] which gives the Laplace transform of a Lévy distribution

$$\int_0^{+\infty} \mathcal{L}_{\alpha,-1}(T) \exp(-sT) dT = \exp(-s^\alpha/C), \qquad (39)$$

with $s = k^2/2m + \imath 0$, C characterizing the width of the temperature distribution and m standing for the emitters mass. The apparent VDF is thus found to be a symmetrical Lévy distribution of indexes $\alpha' = 2\alpha$ and $\beta' = 0$

$$f_a(v) = \frac{1}{v_\alpha}\mathcal{L}_{2\alpha,0}\left(\frac{v}{v_\alpha}\right). \qquad (40)$$

where $v_\alpha = (C^{1/\alpha}/2m)^{1/2}$. For example, for $\alpha = 0.5$ the apparent VDF (i.e. the Doppler line shape) is therefore a Lorentzian. The whole line is thus affected by temperature fluctuations in this case, because of the very fat tails of the temperature PDF. Asymptotically,

$$f_a(v) \sim \frac{1}{|v|^{2\alpha+1}}, \qquad (41)$$

in accordance with equation (37). Here, the value of α is such that $1 < 2\alpha + 1 < 3$ and therefore spans a different range than in the Sinai model.

6.4 Discussion of the results

The study of the case where only one variable fluctuates leads to several enlightening conclusions. First of all, the Doppler profile is only affected by ion temperature and fluid velocity fluctuations along the line of sight, in contrast to the line brightness which essentially reflects the variations of the density. The line width, i.e. its second moment, is essentially affected by velocity fluctuations, the effect being more significant for heavy emitters. For hydrogen lines, velocity fluctuations can therefore be neglected if the study is restricted to the core of the line, as is usually done [9,11,12], whenever the fluctuation rate is such that $\sigma_u/v_{th} \lesssim 30\%$. Temperature fluctuations having long wings PDFs might also affect the bulk of the line, as exemplified by the one sided Lévy PDF case. The most conspicuous modifications occur on Doppler line wings, which are significantly altered by turbulent velocity or temperature fluctuations having non-Gaussian PDFs. More precisely, long tails for the PDF translates into long tails for the apparent VDF, i.e. slowly decreasing line wings. In this sense, modifications on line wings are associated to intermittency. The approach proposed here could give precious information on the asymptotical behavior of the temperature fluctuations PDF, by allowing to check theoretical or numerical predictions. At the very least, it should provide an upper bound to the temperature PDF's tails, which can play an essential role in transport estimates. The results thus obtained could be cross-checked using High Frequency Charge Exchange Recombination Spectroscopy (HF-CHERS) [14], from which time series of ion temperature fluctuations, and hence their PDF, can be measured on the relevant time scales. This technique provides more direct measurements, at the expense of a more complicated experimental set-up which is not currently implemented on any fusion device. Since the technique proposed in this work is quite indirect, significant modeling efforts are required to analyze the data. On the other hand, its experimental implementation requires only rather mild improvements of otherwise routine spectroscopy diagnostics. The practical aspects are discussed in details in the next section.

6.5 Experimental implementation

In this section, we first discuss the experimental relevance of the results presented in this work, and then the modeling required to analyze the data.

Let us first comment on the Tore Supra spectra which we have mentioned in the introduction, and which prompted this work [20]. The measured Dα spectra displayed marked deviations from Gaussianity in the far line wings, which were consistent with a power law behavior. However, since these results were obtained as a by product of routine measurements, the experimental conditions (i.e. discharge characteristics and measurement chain) were not optimized for line wings determination. As a result, while clearly showing the existence of deviations from the expected behavior in line wings, these experiments where not entirely conclusive with respect to their wavelength functional dependence. Increasing by one order of magnitude the dynamic range of the measurements would allow to draw definite conclusions. We show in the following that this can be achieved by performing discharges with longer stationary phases to reduce noise in the data, and by implementing tailored binning techniques in the CCD readout. In fact, our formalism is valid for long integration times, whose value is in practice limited by the actual duration of the discharge stationary phase during which the measurements are performed. However, the intensity of the Dα line is high enough so that excellent signal to noise ratios (SNR) can be achieved with a high spectral

resolution and acquisition times of the order of one second, so that this is not a stringent constraint. Therefore, the actual limitations are to be found in the spectrometer itself, namely stray light which could limit the intra-spectral dynamic range, and the dynamical range of the CCD. The former manifests itself in the tails of the apparatus function, which have to be carefully measured. Indeed, even for an idealized spectrometer (i.e. neglecting aberrations and scattering at the surfaces of optical elements), diffraction is unavoidable and leads to a slow decrease of the apparatus function [37]. For CCDs, dynamic ranges of four orders of magnitudes, corresponding to a 16 bits AD (Analog to Digital) converter, are commonly available (this was used for the Tore Supra measurements). This gives the dynamic range achievable during one exposure of the CCD, and can be further improved by averaging successive exposures. If the most important source of noise comes from the readout process (this happens for low intensities, e.g. in the wings), it is better in terms of SNR to increase the acquisition time τ_m instead of averaging N spectra with shorter acquisition times τ_m/N, while the two solutions are equivalent if photon shot noise dominates. The best way to proceed would therefore be to choose the acquisition time large enough so that the full dynamic range is used, and then average over as much similar frames as possible. Saturation in the center of the line should be avoided because of charge blooming, and in order to fully take advantage of the detector dynamics, the later should be cooled as much as necessary so as to reduce dark currents to the lowest achievable level. For integration times of the order of one second, the latter can in practice be reduced to insignificant levels, that is smaller than the readout noise. If needed, tailored charge binning procedures, i.e. summing charge from adjacent pixels prior to readout, can be implemented [43]. These can considerably improve the dynamical range of the detector when the binning factor in the direction parallel to the spectrometer slit height is determined from the intensity [43,44]. The idea there is to reduce the number of pixels binned in the slit height direction where the intensity is large, so as to avoid saturation of the serial register or the output node of the CCD. Conversely, for low intensities binning over all available pixels is performed. If the minimum meaningful detection level is defined by a SNR value of 5, which would typically correspond to 20 counts, and 100 pixels are available in the slit height direction, with a 16 bits AD converter the intra-spectral dynamic range would be of the order of 3×10^5 instead of 3×10^3. Hence, measuring line shapes over 4–5 orders of magnitude in intensity with a SNR of 5 at the lower end of the intensity range is experimentally achievable with existing techniques. Further improvement of the SNR can be obtained by averaging successive frames.

Now we come to the Tokamak setting of the measurements. First, it should be pointed out again that in edge plasmas there exists a regime where Doppler broadening is dominant in the line wings, and that this regime is in principle experimentally accessible. Moreover, there is no strong impurity line which falls in the blue wing ($\lambda < \lambda_0$) of Dα. In particular, the contribution of the He II Brβ line at $\lambda_0 = 6560.1$ Åis negligible, unless large quantities of helium are injected [45], and O II lines are also too weak to be observed in normal operation. This has been illustrated by the measurements performed in the Tore supra Tokamak [20], were no strong disturbances were seen. Next, let us discuss the modeling aspects. The analysis would proceed by forward modeling, i.e. by comparison between a Doppler profile calculated assuming a given PDF for the turbulence, and the experimental profile. Firstly, comparing to an experimental spectra requires to reconstruct the total spectra, that is to include contributions of the classes of neutrals which are not locally created by charge exchange, as mentioned in Section 3.1. This can be done most accurately by using a neutral transport code, e.g. EIRENE [46], which solves the Boltzmann equation for the neutral VDF retaining the relevant atomic processes in a realistic geometry. The influence of turbulent fluctuations on these classes of neutrals is much weaker. In fact, the VDF of neutrals created by molecular dissociations is only very weakly sensitive to the edge plasma parameters [47] (unless the changes are drastic, such after gas puffing, a situation which is excluded here), and fluctuations in the inner plasma have a much smaller amplitude than in the edge, and thus does not significantly affect the VDF of neutrals created by charge exchange there. Such an approach would also allow to properly take into account integration along the line of sight. The latter effect can however be starkly reduced if the line of sight is carefully chosen. The overall accuracy of such a calculation essentially depends on the extent to which the plasma profiles are known. It can be estimated by varying these input parameters, and depends on the detailed experimental settings. The uncertainties on the plasma parameter are reasonable, since the plasma profiles are routinely measured using Thompson Scattering, Electron Cyclotron Emission, Reflectometry and Recombination Charge Exchange Spectroscopy, e.g. [48,49].

Finally, we come to the modeling of turbulent fluctuations. The first problem to address is the relevance of the approximation retaining only one fluctuating parameter. Measurements performed in the so-called TFTR supershot discharges have shown that parallel velocity fluctuations rates are almost one order of magnitude smaller than ion temperature fluctuations [14]. This suggests that, at least for these kind of discharges, when the LOS is parallel to the magnetic field, ion temperature fluctuations should have a dominant effect on line shapes, hence justifying the neglect of all other fluctuations. If velocity fluctuations measurements are not available, the most straightforward way to give theoretical ground to this approximation would be to rely on numerical integration of a set of fluid equations describing edge turbulence and including ion temperature fluctuations, which would allow calculation of the apparent VDF from equation (15). The ion temperature PDF could be obtained from the same simulation, and then used to recompute the apparent VDF from equation (33). More generally, equation (13) allows the calculation of the profile for any PDF obtained from numerical or analytical calculations.

7 Apparent non-Boltzmann statistics

For the sake of simplicity, let us only consider temperature fluctuations here. The fact that the apparent VDF can be a Lévy distribution highlights a connection between spectroscopy, turbulence and anomalous statistics involving power-law tails, such as the Lévy statistics. Indeed, it should be emphasized that in the case where no other observable than the spectral line shape is available (e.g. in Astrophysics), it is by no mean possible to determine whether the observed plasma is actually turbulent or homogeneous. Therefore, if the temperature PDF is a Lévy distribution $\mathcal{L}_{\alpha,-1}(T)$, the Doppler spectra might be interpreted as resulting from an homogeneous and stationary plasma governed by Levy statistics. In other words, everything happens as if the plasma under study were in a non-equilibrium stationary state characterized by the Lévy distribution of equation (40). This stationary state can be seen as resulting from a relaxation process governed by the following Fractional Fokker-Planck Equation (FFPE) [20,50,51]

$$\frac{\partial f_a(v,t)}{\partial t} = \bar{\nu}\frac{\partial}{\partial v}[v f_a] + \bar{D}\frac{\partial^{2\alpha} f_a}{\partial |v|^{2\alpha}}. \tag{42}$$

where $\bar{\nu}$ and $\bar{D}$ are such that $\bar{D}/\bar{\nu} = 2\alpha c/(2m)^{\alpha}$. Here, the fractional derivative is defined in the sense of Riesz [42]

$$\frac{\partial^{2\alpha} f_a}{\partial |v|^{2\alpha}} = TF^{-1}\left[-|k|^{2\alpha}\tilde{f}_{\mathit{eff}}\right]. \tag{43}$$

The usual Fokker-Planck equation (FPE) is recovered for $\alpha = 1$. In our case $\alpha < 1$, and the apparent VDF cannot be Gaussian. The main physical difference between the FPE and the FFPE given by equation (42) is the spatial non locality of the latter, obvious from the definition of the fractional derivative. This non locality is a consequence of the existence of flights connecting distant regions in the velocity space (the so-called Lévy flights). This property can be traced back to the underlying description of the turbulent plasma. Indeed, at the microscopical scale the trajectory of the radiators can be modelled by a Langevin equation with Gaussian white noise [52,53]. This model describes the collisional relaxation of the local velocity distribution toward the local Maxwellian equation (8). Using the fluctuation-dissipation theorem and the expression of the diffusion coefficient stemming from a random walk model [53] leads to

$$\frac{\langle \Delta v^2 \rangle}{\tau_j} \sim \nu \frac{k_B T}{m}, \tag{44}$$

where T is the local temperature and τ_j the typical time between two jumps in the velocity space. Temperature thus determines the characteristic size of jumps in the velocity space. Therefore, high probabilities for large temperature fluctuations in the actual turbulent plasma imply high probabilities for flights in the apparent velocity space. This provides a simple physical picture explaining why the temperature PDF and the apparent VDF asymptotical behavior are linked, and leads to a deeper understanding of equation (37). Our results are reminiscent of those presented in references [52,54,55], where a similar interpretation of Tsallis non extensive statistical mechanics occurrence was proposed. The latter case arises if the temperature PDF is such that $1/T$ is gamma distributed [54]. Let us emphasize that in our model, the temperature PDF shape is not arbitrary. In fact, it has to be determined from the fluid equation satisfied by the temperature field in the plasma under consideration, in which relevant expressions for both the source term and the flux have to be specified (see Eq. (7)). For each of these expressions, the non-linear character of the latter equation should give rise to a different non-Gaussian statistical behavior, i.e. lead to a specific PDF, and therefore to a particular apparent statistics. A natural extension of this work would be to determine what properties fluid equations should have so as to lead to a Lévy distribution for temperature.

8 Conclusion and perspectives

In this paper, we have presented a model retaining low frequency turbulence in Doppler line shape calculations. This approach is in particular relevant to the modeling of lines routinely measured in edge plasmas of fusion devices. We have shown that in presence of low frequency turbulence, a straightforward analysis of Doppler profiles yields an apparent velocity distribution function. This apparent VDF is a spatial and time average of the local VDF. To investigate its shape, we have used a statistical description of the plasma turbulent fluctuations, relevant whenever the acquisition time of the spectrometer is large with respect to the typical turbulent time scale. The resulting expression for the apparent VDF involves the joint Probability Density Function of the fluctuating fields. Next, considering the case where only one variable fluctuates, we have obtained several new results. While density fluctuations do not affect Doppler line shapes, velocity or ion temperature fluctuations can influence line shapes, and in particular line wings. This is especially the case when their PDF have long tails such as power laws. It might therefore be possible to diagnose such a behavior by the mean of line shapes, once Stark effect has been carefully ruled out. A reliable comparison with experiments would imply dedicated measurements which are not yet available, but also further modeling. In particular, the use of a turbulence code would be very helpful for diagnosis purposes, and this possibility will be investigated in a future work. From a more fundamental point of view, our work sheds light on some possible connections between turbulence, spectroscopy and non Boltzmann statistics, such as those involving Lévy or Tsallis distributions. Our approach furthermore relates the occurrence of one of these particular statistics to the properties of the fluid equations describing turbulence. It thus provides a frame to investigate both experimentally and theoretically some of the fundamentals aspects of the statistical properties of the physical observables in out of equilibrium plasmas.

Appendix A: Lévy distributions

We present here the definitions of the various Lévy distributions used in this work. These distributions cannot in general be expressed analytically, but their Fourier transform can. The following convention for the inverse Fourier transform will be used

$$f(x) = \frac{1}{2\pi}\int_{-\infty}^{+\infty} \tilde{f}(k)\exp(-ikx). \tag{45}$$

In the Fourier space, the Lévy distribution $L_{\alpha,\beta}(x)$ is given by

$$\ln \tilde{L}_{\alpha,\beta}(k) = -C|k|^{\alpha}\left(1 + i\beta\frac{k}{|k|}\omega(k,\alpha)\right), \tag{46}$$

where C controls the width of the distribution, and the function $\omega(k,\alpha)$ is defined by

$$\begin{aligned}\omega(k,\alpha) &= \tan(\pi\alpha/2) \quad \text{for } \alpha \neq 1,\\ &= (2/\pi)\ln|k| \quad \text{for } \alpha = 1.\end{aligned} \tag{47}$$

α is called the index of the distribution , and takes the values $0 < \alpha < 2$. To avoid overly cumbersome notations, we do not label $L_{\alpha,\beta}$ with C, but it should be kept in mind that the latter can assume any arbitrary positive value (this notation differs from the one we used in Ref. [19], where $C = 1$ was implied). The parameter β is such that $-1 < \beta < 1$, and controls the asymmetry of the distribution. In fact, Lévy distributions are symmetric for $\beta = 0$, and one sided for $\beta = \pm 1$. For $\beta = -1$, the distribution is non zero for $x > 0$ when the convention of equation (45) is adopted. The limiting case $\alpha = 2$ and $\beta = 0$ corresponds to the Gaussian distribution, but there is no smooth transition as $\alpha \to 2^{-}$. In particular, for x large

$$L_{\alpha,\beta}(x) \sim \frac{A_{\alpha,\beta}}{|x|^{\alpha+1}}. \tag{48}$$

Lévy distributions have an infinite variance, as can easily be checked in the Fourier space or from their asymptotic behavior. A possible remedy for this generally unphysical feature is to introduce a cut-off of the power-law behavior in the tails of the distribution. This procedure leads to the so called truncated Lévy flights, whose PDF retains an analytical form in the Fourier space in the version proposed in reference [41]. In the symmetric case, the corresponding characteristic function is given by

$$\begin{aligned}\ln \tilde{P}_{\alpha,\lambda}(k) = &\frac{C}{\cos\left(\frac{\pi\alpha}{2}\right)}\\ &\times\left[\lambda^{\alpha} - (k^2+\lambda^2)^{\frac{\alpha}{2}}\cos\left(\alpha\arctan\frac{|k|}{\lambda}\right)\right],\end{aligned} \tag{49}$$

where λ is the cutoff parameter. The variance σ of the PDF is obtained from the second derivative of the characteristic function, which yields

$$\sigma^2 = \frac{\alpha(\alpha-1)}{\lambda^{2-\alpha}\cos(\pi\alpha/2)}C \tag{50}$$

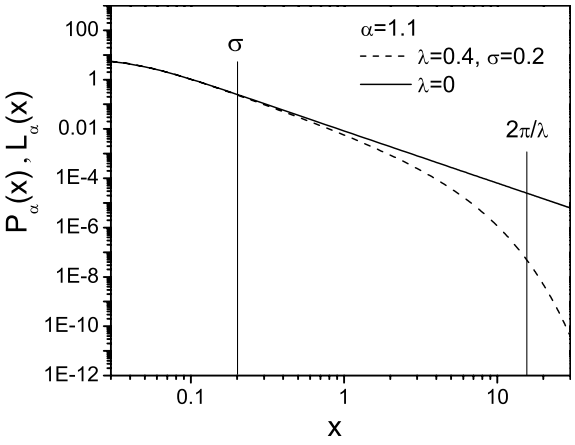

Fig. 8. Comparison between the truncated Lévy flight PDF $P_{\alpha}(x)$ with $\alpha = 1.1$, $\lambda = 0.4$ and $\sigma = 0.2$ and the limiting Lévy distribution corresponding to $\lambda \to 0$.

In the limit $\lambda \to 0$, the usual symmetric Lévy distribution is recovered, and $\sigma \to +\infty$. For any given σ, the characteristic function reduces to that of a Lévy distribution for $k \gg \lambda$, and to that of a Gaussian for $k \ll \lambda$. The wings of the PDF $P_{\alpha,\lambda}(x)$ are therefore Gaussian for $x \gg 2\pi/\lambda$, thus ensuring the convergence of its moments. An illustration of this behavior is provided on Figure 8, where the truncated Levy flight PDF $P_{\alpha,\lambda}(x)$ calculated for $\alpha = 1.1$, $\sigma = 0.2$ and $\lambda = 0.4$ is compared to the corresponding Lévy distribution. Note that if $\lambda > 2\pi/\sigma$, the PDF becomes essentially Gaussian.

The authors would like to thank F.B. Rosmej and R. Guirlet for helpful discussions. This work is part of a collaboration (LRC DSM 99-14) between the Laboratoire de Physique des Interactions Ioniques et Moléculaires and the Département de Recherches sur la Fusion Contrôlée, CEA Cadarache.

References

1. J.A. Krommes, Phys. Rep. **360**, 1 (2002)
2. X. Garbet, Plasma Phys. Control. Fusion **43**, A251 (2001)
3. W. Horton, Rev. Mod. Phys. **71**, 735 (1999)
4. H.R. Griem, *Spectral Line Broadening by Plasmas* (Academic Press New York and London, 1974)
5. E. Oks, *Plasma Spectroscopy* (Springer-Verlag, Berlin Heidelberg, 1995)
6. H. Capes, D. Voslamber, Phys. Rev. A **15**, 1751 (1977)
7. C. Deutsch, G. Bekefi, Phys. Rev. A **14**, 854 (1976)
8. M. Baranger, B. Mozer, Phys. Rev. **123**, 25 (1961)
9. H. Kubo, H. Takenaga, T. Sugie, S. Higashijima, S. Suzuki, A. Sakasai, N. Hosogane, Plasma Phys. Control. Fusion **40**, 1115 (1998)
10. D.P. Stotler, C.H. Skinner, R.V. Budny, A.T. Ramsey, D.N. Ruzic, R.B. Turkot Jr, Phys. Plasmas **3**, 4084 (1996)
11. J.D. Hey, C.C. Chu, E. Hintz, J. Phys. B: At. Mol. Opt. Phys. **32**, 3555 (1999)
12. M. Koubiti, Y. Marandet, A. Escarguel, H. Capes, L. Godbert-Mouret, R. Stamm, C. De Michelis, R. Guirlet, M. Mattioli, Plasma Phys. Control. Fusion **44**, 261 (2002)

13. N. Bretz, Rev. Sci. Instrum. **68**, 2927 (1997)
14. H.T. Evensen, R.J. Fonck, S.F. Paul, G. Rewoldt, S.D. Scott, W.M. Tang, M.C. Zarnstorff, Nucl. Fusion **38**, 237 (1998)
15. R. Jha et al., Phys. Plasmas **10**, 699 (2003)
16. G.M. Zaslavsky, M. Edelman, H. Weitzner, B. Carreras, G. McKee, R. Bravenec, R. Fonck, Phys. Plasmas **7**, 3691 (2000)
17. M. Jakubowski, R.J. Fonck, G.R. Mckee, Phys. Rev. Lett. **89**, 265003 (2002)
18. Y. Marandet, P. Genesio, M. Koubiti, L. Godbert-Mouret, B. Felts, R. Stamm, H. Capes, R. Guirlet, Nuc. Fus. **44**, S118 (2004)
19. Y. Marandet, H. Capes, L. Godbert-Mouret, M. Koubiti, R. Stamm, Europhys. Lett. **69**, 531 (2005)
20. Y. Marandet, H. Capes, L.Godbert-Mouret, R. Guirlet, M. Koubiti, R. Stamm, Commun. Non Lin. Sci. Num Simul. **8**, 469 (2003)
21. S.I. Braginskii, Rev. Plasma Phys. **1**, 205 (1965)
22. F. Hinton, R. Hazeltine, Rev. Mod. Phys. **48**, 239 (1976)
23. R.K. Janev, D. Reiter, U. Samm, *Collision Processes in Low-Temperature Hydrogen Plasmas*, Jül-Bericht 4105, Forschungszentrum Jülich, 2003
24. F.B. Rosmej, H. Capes, M. Koubiti, V.S. Lisitsa, Y. Marandet, A. Meigs, R. Stamm, Europhys. Conf. Abstr. **27A**, 1.176 (2003)
25. S.G. Rautian, I.I. Sobel'man, Sov. Phys. Usp. **9**, 701 (1967)
26. B.H. Bransden, C.J. Joachain, *Physic of atoms and molecules* (Longman Scientific and Technical, 1983)
27. Y. Marandet, H. Capes, L. Godbert-Mouret, M. Koubiti, R. Stamm, R. Guirlet, *Spectral Line Shapes*, edited by C.A. Back, Vol. 12, AIP, Volume 645, page 60, 2002
28. U. Frisch, *Turbulence* (Cambridge University Press, 1995)
29. A. Das, P. Kaw, Phys. Plasmas **2**, 1497 (1995)
30. S.B. Pope, *Turbulent Flows* (Cambridge University Press, 2000)
31. H. Chen, S. Chen, R.H. Kraichnan, Phys. Rev. Lett. **63**, 2657 (1989)
32. Y.G. Sinai, V. Yakhot, Phys. Rev. Lett. **63**, 1962 (1989)
33. R.T. Pierrehumbert, Chaos **10**, 61 (2000)
34. D.R. Fereday, P.H. Haynes, Phys. Fluids **16**, 4359 (2004)
35. C. Tsallis, Chaos **6**, 539 (1995)
36. H.R. Griem, *Principles of Plasma Spectroscopy*, Cambridge Monographs on Plasma Physics (Cambridge University Press, 1997)
37. A. Unsöld, *Physik des Sternatmosphären* (Springer-Verlag, Berlin, 1955)
38. N.A. Iganov, R.A. Sunyaev, Astron. Lett. **29**, 791 (2003)
39. M.D. Ding et al., Astron. Astrophys. **348**, L29 (1999)
40. Ying Liu, Ming-De Ding, Chin. J. Astron. Astrophys. **2**, 277 (2002)
41. I. Koponen, Phys. Rev. E **52**, 1197 (1995)
42. W. Paul, J. Baschnagel, *Stochastic processes, From Physics to finance* (Springer-Verlag, 1999)
43. *Charge-Transfer Devices in Spectroscopy*, edited by J.V. Sweedler, K.L. Ratzlaff, M.B. Denton (VCH, 1994)
44. P.M. Epperson, M.B. Denton, Anal. Chem. **61**, 1513 (1989)
45. R. Guirlet et al., Plasma Phys. Control. Fusion **43**, 177 (2001)
46. D. Reiter, M. Baelmans, P. Börner, Fus. Sci. Technol. **47**, 172 (2005)
47. J.D. Hey, C.C. Chu, Ph. Mertens, J. Phys. B:At. Mol. Opt. Phys. **38**, 3517 (2005)
48. S. Brezinsek et al., Fus. Sci. Technol. **47**, 209 (2005)
49. A.J.H. Donné et al. Fus. Sci. Technol. **47**, 220 (2005)
50. S. Jespersen, R. Metzler, H.C. Fogedby, Phys. Rev. E **59**, 2736 (1999)
51. A.V. Chechkin, V. Yu. Gonchar, Phys. Plasmas **9**, 78 (2002)
52. C. Beck, Phys. Rev. Lett. **87**, 180601 (2001).
53. P. Resibois, M. DeLeener, *Classical Kinetic Theory of fluids* (Wiley-Interscience, 1977)
54. G. Wilk, Z. Wlodarczyk, Phys. Rev. Lett. **84**, 2770 (2000)
55. C. Beck, E.D.G. Cohen, Physica A **322**, 267 (2003)